Inorganic Chemistry

Article

pubs.acs.org/IC

Synthesis and Structure Determination of $CaSi_{1/3}B_{2/3}O_{8/3}$: A New Calcium Borosilicate

Emmanuel Véron,*[,†,‡] Mounesha N. Garaga,[†,‡] Denis Pelloquin,[§] Sylvian Cadars,[†,‡] Matthew Suchomel,[⊥] Emmanuelle Suard,[∥] Dominique Massiot,[†,‡] Valérie Montouillout,[†,‡] Guy Matzen,[†,‡] and Mathieu Allix*[,†,‡]

[†]CNRS, UPR3079 CEMHTI, 1D Avenue de la Recherche Scientifique, 45071 Orléans Cedex 2, France

[‡]Université d'Orléans, Avenue du Parc Floral, BP 6749, 45067 Orléans Cedex 2, France

[§]ENSICAEN, UMR 6508 CRISMAT, 6 Boulevard du Maréchal Juin, 14050 Caen Cedex4, France

[∥]Institute Max von Laue and Paul Langevin, BP156, 38042 Grenoble, France

[⊥]Advanced Photon Source, Argonne National Laboratory, Argonne, Illinois 60439, United States

Supporting Information

ABSTRACT: This article reports on the identification, synthesis, and in-situ structure determination of a new crystalline calcium borosilicate compound of composition $CaSi_{1/3}B_{2/3}O_{8/3}$. Synthesis was carried out by complete crystallization on annealing from a corresponding glassy composition in the widely studied $CaO-SiO_2-B_2O_3$ ternary system. The crystallographic structure was determined ab initio using electron diffraction information and the charge flipping algorithm performed on synchrotron and neutron powder diffraction data collected in situ at high temperature. $CaSi_{1/3}B_{2/3}O_{8/3}$ is found to crystallize in the $Pna2_1$ (no. 33) orthorhombic space group, with a = 12.1025(4) Å, b = 5.2676(1) Å, c = 3.7132(1) Å, and V = 236.71(1) Å^3 at 650 °C. Solid-state ^{29}Si and ^{11}B NMR experiments have confirmed the existence of finite chains along the c axis, formed by corner-sharing SiO_4 tetrahedra and BO_3 units. Silicon and boron species share a crystallographic site, and the Si/B distribution induces different possible arrangements of the chains which are discussed in light of DFT calculations. At room temperature, the existence of a superstructure, resulting from the ordering within nanoscale domains, was explored by transmission electron microscopy.

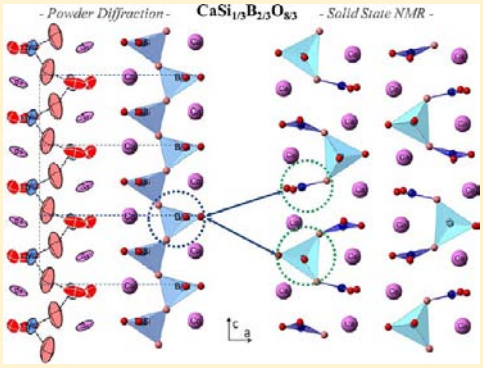

INTRODUCTION

Boron and alkali and alkaline earth oxides are key additives used to tune properties in technologically important glass materials such as bioactive, optical, and thermal shock-resistant glasses. In particular, boron oxide is known to greatly decrease solidus temperatures of complex oxides and thus classically added to the glass compositions in order to optimize melting and forming.[1]

However, despite their importance within the mineralogy, glass, and ceramic communities,[2−5] only a few calcium borosilicate crystalline phases have been reported in the literature. To date, only the danburite ($CaB_2Si_2O_8$)[6] and okayamalite ($Ca_2B_2SiO_7$)[7,8] mineral structures have been described in the literature as part of the ternary diagram. Both structures consist of tetrahedral frameworks with ordered BO_4 and SiO_4 tetrahedra which accommodate Ca in irregular polyhedra. In addition, the partial solid solution of B_2O_3 in Ca_2SiO_4 occurring along the $Ca_2SiO_4-Ca_3B_2O_6$ tie line, represented by the formula $Ca_{2-0.5x}(SiO_4)_{1-x}(BO_3)_x$ ($0 < x \leq 0.33$), has been studied in detail by Fletcher and Glasser.[9] This ternary system contains the $Ca_{11}B_2Si_4O_{22}$ compound, previously observed by Suzuki and Hira,[10] which is stable up to its liquidus temperature at 1420 °C.

The suggestion of a new unknown calcium borosilicate phase was first made by Bauer[11] in a 1962 study of boron substitution for aluminum in the naturally occurring mineral gehlenite ($Ca_2Al_2SiO_7$). This work reports an extensive solid solution with incorporation of up to 60 atom % boron content in the structure. Additionally, the authors also note the presence of an unknown compound, which they denote "X phase", located in the boron-rich region of the $Ca_2Al_2SiO_7-Ca_2B_2SiO_7$ pseudo-binary diagram.

In the present study, we synthesized this crystalline "X-phase" compound in the $CaO-B_2O_3-SiO_2$ ternary system and determined its composition to be $CaSi_{1/3}B_{2/3}O_{8/3}$. A combination of high-temperature neutron and synchrotron powder diffraction data with electron diffraction was used to solve the structure. The local arrangement, and more especially the Si/B ordering, is then described based on data from ^{29}Si and ^{11}B solid-state nuclear magnetic resonance (NMR) experiments

Received: September 28, 2012
Published: January 11, 2013

   dx.doi.org/10.1021/ic302114t | Inorg. Chem. 2013, 52, 4250−4258

and first-principles calculations. Evidence for nanoscale superstructure domains at room temperature from transmission electron microscopy is presented, and the superstructure stability with temperature is investigated by in-situ transmission electron microscopy.

EXPERIMENTAL SECTION

Synthesis. All glass samples were synthesized using $CaCO_3$ (99.95%, Alfa Aesar), Al_2O_3 (99.99%, Alfa Aesar), SiO_2 (99.99%, Saint-Gobain), and B_2O_3 (99.99%, Alfa Aesar). The hygroscopic B_2O_3 precursor was previously dried, and the starting oxides were weighted in a glovebox under argon atmosphere to avoid moisture contamination. Glass melting was performed in platinum crucibles at different high temperatures ranging from 1200 to 1500 °C depending on the targeted composition. Samples were kept at this temperature for 2 h and subsequently quenched to room temperature. All glass samples were optically clear and in a completely amorphous state as confirmed by powder X-ray diffraction measurements. In order to reduce the neutron absorption of the samples containing ^{10}B by natural abundance, powder samples for powder neutron diffraction experiments were prepared from purified commercial products containing only ^{11}B.

Powder Diffraction. Laboratory X-ray diffraction (XRD) measurements were performed on a D8 Advance Bruker Bragg−Brentano diffractometer (Cu Kα radiation) equipped with a Vantec-1 linear detector. In-situ high-temperature diffraction data were collected on an Anton Paar oven chamber (model HTK1200N). Fine granular powder of the sample was deposited on a platinum disk in an alumina crucible. The temperature behavior and thermal expansion of the setup had previously been calibrated using the corundum reference.[12]

Powder neutron diffraction data were obtained on the D2B diffractometer at the Institute Laue Langevin, located in Grenoble, France. High-resolution data have been collected between 0 and 160° (2θ) for 8 h at 650 °C in a vacuum furnace with vanadium heating elements. Monochromatic radiation (1.59516 Å wavelength) and a 0.05° step size have been used.

High-intensity and high-resolution synchrotron powder diffraction data have been recorded on the 11-BM diffractometer at the Advanced Photon Source (APS), Argonne National Laboratory. Sample powder was loaded in a 0.3 mm diameter quartz capillary and heated at 5 °C/min to 700 °C using a hot-air blower (Cyberstar). Data were collected at 700 °C over the 2θ range of 0.5−40° using a step size of 0.002° and wavelength of λ = 0.412225 Å. The sample was spun at 10 Hz to improve powder averaging of the crystallites.

Density measurements have been conducted on an ACCUPYC 1330 (Micromeritics) gas picnometer running under helium. The temperature of the experiment was kept constant to 30 ± 1 °C. The average density value was obtained by averaging 10 measurements in order to minimize the uncertainty.

Transmission Electron Microscopy (TEM). Synthesized samples were analyzed by electron diffraction (ED) and energy-dispersive spectroscopy (EDS) using a Philips CM20 fitted out with an Oxford EDS analyzer. The high-resolution electron microscopy study was performed on a JEOL 2010F transmission electron microscope (Cs = 1 mm) equipped with a Gatan high-temperature sample holder (model 901) working from RT to 1000 °C. Samples to be observed were first crushed in ethanol, and a drop of the solution with the small crystallites in suspension was deposited onto a carbon-coated copper grid.

Nuclear Magnetic Resonance (NMR). The quantitative ^{29}Si solid-state magic angle spinning (MAS) NMR experiment was performed at room temperature on a 4.7 T Bruker Avance I wide-bore spectrometer using a 7 mm MAS probehead at a Larmor frequency of 39.75 MHz. The signal was accumulated over 648 transients with a 3600 s recycling delay at a spinning frequency of 5 kHz. The ^{11}B solid-state echo-MAS NMR spectrum was recorded on a 9.4 T Bruker Avance I spectrometer at a Larmor frequency of 128.37 MHz using a 4 mm double-resonance (^{19}F-X) probehead. Low-power-selective 90° and 180° pulses of 11 and 22 μs were used to excite the central transition. Sample was spun at a MAS frequency of 14 kHz, and signal enhancement was achieved by means of a double-frequency sweep (DFS) preparation.[13] Signal was accumulated over 2048 transients with a relaxation delay of 1 s. The two-dimensional ^{11}B z-filtered MQ-MAS[14,15] NMR spectrum was collected on a 9.4 T Bruker Avance I spectrometer using a 4 mm DR (^1H-X) probehead. Excitation and conversion pulse lengths were optimized to 3.4 and 1.2 μs, respectively. Sample was spun at a MAS frequency of 14 kHz. A selective 90° pulse of 12 μs was utilized to bring back magnetization to the z axis before acquiring the signal. A z-filter delay of 0.35 ms was used. Signal was acquired over 24 scans for each of 192 increments with a separation delay of 1 s. Chemical shifts were externally referenced to a 1 M aqueous solution of BF_3OEt_2 and tetramethylsilane for ^{11}B and ^{29}Si, respectively. Deconvolutions of NMR spectra were achieved with the Dmfit program.[16]

DFT Calculations. First-principles calculations with periodic boundary conditions were achieved using the CASTEP code,[17,18] which relies on a plane-wave-based density functional theory (DFT) approach. Electron correlation effects are modeled using the Perdew−Burke−Ernzerhof (PBE) generalized gradient approximation (GGA).[19] For geometry optimizations we employed a planewave cutoff energy of 650 eV and the default "on-the-fly" ultrasoft[20] pseudopotentials of CASTEP 5.5, except for calcium, whose potential must be modified to avoid errors on the calculated response of surrounding atoms (as described in the Supporting Information, Table S1).[21,22] Convergence thresholds were set to 5×10^{-6} eV/atom for the total energy, 1×10^{-2} eV/Å for the maximum ionic force, and 5×10^{-4} Å for the maximum ionic displacement. NMR calculations were performed using the gauge including projector augmented wave approach (GIPAW)[23,24] at the same cutoff energy of 650 eV, which led to calculated ^{11}B and ^{29}Si NMR shieldings converged within less than 0.1 ppm. Calculations were conducted on supercells consisting in 1 × 1 × 3 or 1 × 1 × 6 original (average) cells (a = 12.086 Å, b = 5.2613 Å, and c = 11.1252 or 22.2504 Å, respectively) using 3 × 5 × 3 and 3 × 5 × 1 Monkhorst−Pack[25] (MP) grids to sample the Brillouin zone, respectively. Detailed descriptions of the model-building procedures are provided in Figure SI5, Supporting Information

RESULTS AND DISCUSSION

Synthesis. According to the pseudo-binary phase diagram published by Bauer,[11] the X phase is observed in the boron-rich region of the $Ca_2Al_2SiO_7$−$Ca_2B_2SiO_7$ gehlenite solid solution (Supporting Information, Figure SI1a). In order to isolate and identify this otherwise unknown compound, in-situ high-temperature laboratory X-ray diffraction studies and a differential scanning calorimetry (DSC) analysis have been performed, starting from a quenched glass sample with the $2CaO-0.2Al_2O_3-0.8B_2O_3-SiO_2$ composition. While heating, the first powder diffraction peaks matching the reported X-phase reflections appeared around 740 °C, in good agreement with DSC data. The existence of some remaining glass in the sample is evidenced by the presence of a broad diffuse background signature in the powder diffraction data. Attempts to identify this phase using the ICDD JCPDF database[26] were unsuccessful. At 810 °C, formation of some boron-substituted gehlenite ($Ca_2Al_{0.4}B_{1.6}SiO_7$) was observed at the expense of the X phase, which effectively disappears with additional heating up to 955 °C (Supporting Information, Figure SI1b).

Compositional information on the X phase was obtained from a transmission electron microscopy (TEM) study undertaken on a glass sample first annealed at 750 °C and then quenched to room temperature. TEM imaging (see example in Supporting Information, Figure SI2) shows crystals with a size of several hundred nanometers lying within a glass matrix. Energy-dispersive X-ray spectroscopy measurements performed in the crystalline regions revealed the presence of

dx.doi.org/10.1021/ic302114t | Inorg. Chem. 2013, 52, 4250−4258

boron, calcium, and silicon with a Ca/Si ratio close to 3 but no aluminum (Supporting Information, Figure SI2). Unfortunately, EDS measurements did not allow quantification of boron due to its too low energy (K_α(B) = 0.18 KeV). To determine its correct content, a series of glasses with variable amounts of boron assuming a Ca/Si ratio fixed to 3 was synthesized (glass melting adjusted between 1400 and 1500 °C) and their crystallization followed in situ by XRD (Supporting Information, Figure SI3). The optimal nominal content of boron to obtain pure X phase has been determined as 22 mol %, suggesting a $CaSi_{0.33}B_{0.75}O_{2.79}$ nominal composition. Interestingly, this new compound is located on the tie line between the $CaSiO_3$ and the $Ca_2B_2O_5$ phases[27] in the CaO-SiO_2−B_2O_3 ternary diagram[9] and represents only the fourth reported calcium borosilicate oxide phase (Figure 1a).

Cell Indexation. To obtain initial crystallographic information, electron diffraction analysis was performed on several crystallites from the $CaSi_{0.33}B_{0.75}O_{2.79}$ sample which was formed by crystallization at 700 °C from the 58.5CaO−19.5SiO_2−$22B_2O_3$ glass sample and quenched at room temperature. Reconstruction of the reciprocal space obtained by tilting around the crystallographic axes exhibits an orthorhombic cell with $a \approx 12.1$ Å, $b \approx 5.2$ Å, and $c \approx 3.7$ Å. Electron diffraction patterns of the [010] and [001] characteristic planes are shown in Figure 2. No condition limiting the general *hkl* reflections

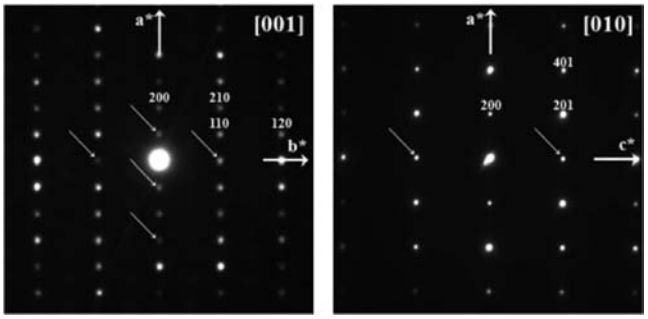

Figure 2. Electron diffraction patterns of the quenched X-phase sample recorded at room temperature along the [001] and [010] directions. Extra *h*00 and 0*k*0 reflections with *h* and *k* = 2*n* + 1 were attributed to double diffraction (white arrows).

was observed during the reciprocal lattice reconstruction, leading to the assignment of a primitive lattice. Two extra conditions 0*kl*, $k + l = 2n$, and *h*0*l*, $h = 2n$, indicate the presence of *n* and *a* glide planes along the *a* and *b* axes, respectively, and restrict the choice of the space group to either *Pnam* or $Pna2_1$. The lattice values and symmetry selection were confirmed for both space groups by good reliability factors of the profile fit (Le Bail method[28]) to the synchrotron powder diffraction pattern obtained in situ at 700 °C. No isostructural compound could be found in the ICSD database using these space groups with similar sets of cell parameters.

Structure Determination. The in-situ high-temperature laboratory X-ray diffraction study showed a systematic broadening of the reflections attributed to the X phase upon cooling back to room temperature (Figure 1b). In order to obtain high-quality data with narrow peak profiles which are required for structure determination, the neutron and synchrotron powder diffraction diagrams were collected in situ at high temperature.

The measured density of 2.82(1) g·cm^{-3} leads to four $CaSi_{0.33}B_{0.75}O_{2.79}$ asymmetric units formula ($Z = 4$). The two possible space groups determined by electron diffraction were introduced in the Superflip[29] program implemented in the Jana[30] software package. The charge-flipping[31] algorithm found in each case a solution from the synchrotron data collected at 700 °C with only two cationic positions for both *Pnam* and $Pna2_1$ space groups and several oxygen positions. For each model, only the cationic sites were retained and refined. Two additional oxygen atoms could be located from Fourier difference maps. The attribution of the Ca and Si species to their corresponding cationic positions was confirmed by Ca−O and Si−O bond lengths within the typical interatomic distance ranges in calcium aluminoborosilicate compounds[32] (2.1−2.5 and 1.5−1.7 Å, respectively). The two models obtained from the synchrotron powder data were then completed with a Rietveld refinement based on neutron powder diffraction data collected in situ at high temperature. The peak shape was modeled by a pseudo-Voigt function using the Thompson−Cox−Hasting[33] formalism. Due to its high neutron scattering length, a third oxygen position then appeared clearly using

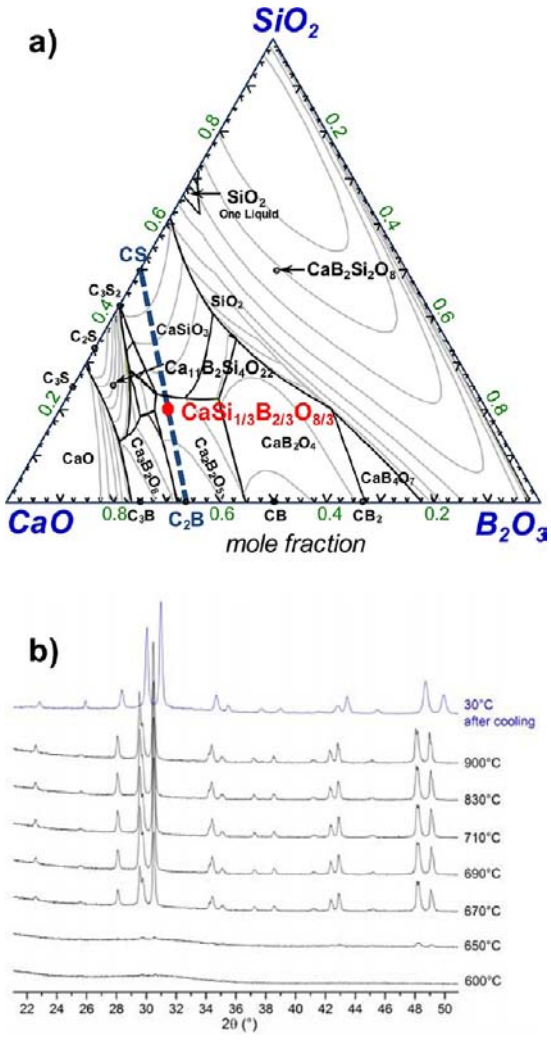

Figure 1. (a) Localization of the new calcium borosilicate oxide (red full circle symbol) in the ternary CaO−SiO_2−B_2O_3 system.[9] (b) In-situ X-ray diffractograms collected while heating (10 °C/min) and starting from a CaO−0.375B_2O_3−0.33SiO_2 glass powder sample. Reflections attributed to the X phase appear from 650 °C. Broadening of these reflections was systematically observed upon cooling at room temperature.

dx.doi.org/10.1021/ic302114t | Inorg. Chem. 2013, 52, 4250−4258

Fourier difference maps. All cationic positions are located on crystallographic sites with 4-fold multiplicity. However, the most symmetric space group, *Pnam*, turned out to be unable to consider any distortion, resulting in inconsistent bond distances. On the other hand, the $Pna2_1$ model, having only general positions (namely, 4*a*), could easily fit the structure by accommodating such distortions, leading to good reliability factors and reasonable bond distances.

At this stage of the structure determination, one calcium, one silicon, and three oxygen atoms were positioned on 4*a* crystallographic sites but no boron atom position could be located in the structure, implying a $CaSiO_3$ cell formula. Furthermore, the Ca:Si ratio of this formula does not concur with the nominal $CaSi_{0.33}B_{0.75}O_{2.79}$ composition, which would require less silicon and oxygen content. A Fourier difference map obtained from a Rietveld neutron refinement of the partial structural model and shown in Figure 3 did not reveal any

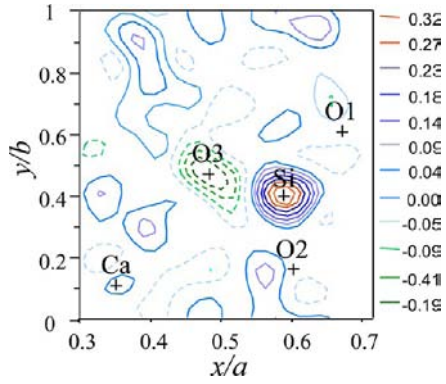

Figure 3. *z*-axis projection (summed between $z = 0$ and 0.4) of the Fourier difference maps performed after Rietveld refinement of the neutron powder diffraction data using 1Ca, 1Si, and 3 O full crystallographic sites as a structural model pattern of the X phase recorded at 650 °C. Residue densities (in arbitrary units) are plotted using 20 levels of contours where solid and broken lines represent positive and negative profiles, respectively. Black crosses indicate atom positions.

additional atomic positions. However, significant negative residual scattering density at the O3 position indicates a partial occupancy of this site, leading to a deficit of density as compared to a model with full occupancies. Similarly, positive residual scattering density at the Si position suggests a mixed Si/B composition, as previously observed for other mineral compounds.[34,35] The higher neutron scattering length of boron-11 (6.65 barns) as compared to Si (4.15 barns) leads to higher density than for the model with pure Si composition, and to positive scattering density on the Fourier difference map.

With this new insight, the cell parameters, atomic positions, anisotropic thermal parameters, and occupancies for all atoms were refined by the Rietveld method leading to the actual $CaSi_{0.33}B_{0.66}O_{2.66}$ (also noted $CaSi_{1/3}B_{2/3}O_{8/3}$) formula. This formula is consistent with the nominal composition ($CaSi_{0.33}B_{0.75}O_{2.79}$) used for synthesis, the slight decrease in boron content (4 mol % of B_2O_3) being attributed to a loss of this volatile element during the initial glass synthesis at high temperature (1500 °C). The corresponding fitted neutron and synchrotron diffraction powder diagrams are shown in Figure 4. Considering the high resolution and high counting level of the data, very good reliability factors (R_{wp} = 3.05%, R_p = 2.30%, χ^2 = 1.57) were obtained. Crystallographic data, final refined

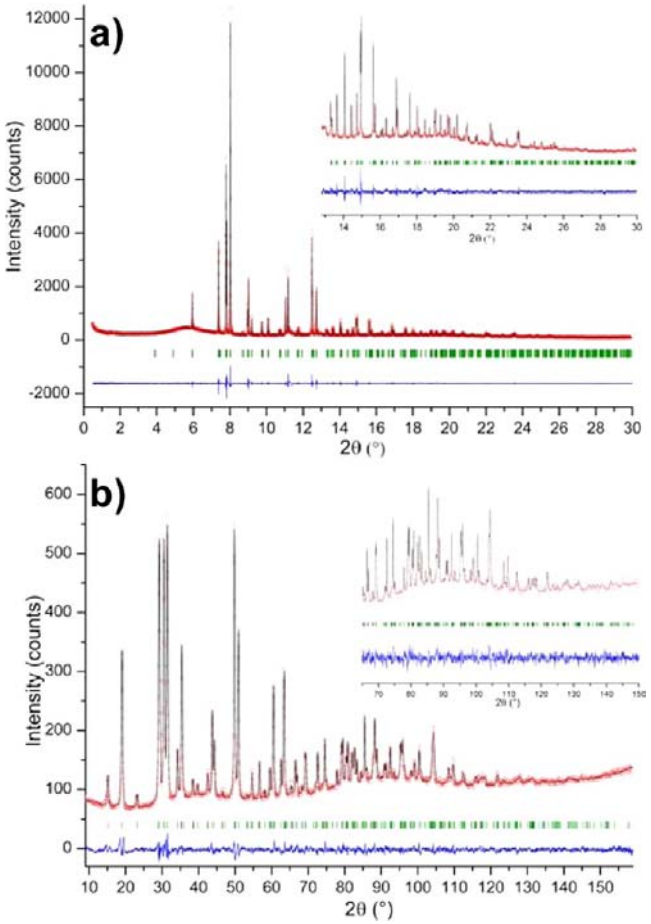

Figure 4. Final Rietveld refinement of (a) synchrotron (R_{wp} = 6.23%, R_p = 4.88%, and χ^2 = 2.13) and (b) neutron (R_{wp} = 3.05%, R_p = 2.30%, and χ^2 = 1.57) powder diffraction data of $CaSi_{1/3}B_{2/3}O_{8/3}$ collected at high temperature. Observed (red circles), calculated (black line), and difference (blue line) profiles are shown. Set of green vertical lines corresponds to reflection positions. Enlargements of the 13−30° and 70−150° angular range (2θ) are embedded.

structural parameters of the new calcium borosilicate phase, and interatomic distances are reported in the Tables 1, 2, and 3.

Table 1. Crystallographic Data Determined for $CaSi_{1/3}B_{2/3}O_{8/3}$ from Neutron Powder Diffraction Data Collected at 650°C

formula	$CaSi_{1/3}B_{2/3}O_{8/3}$
Z	4
cryst syst	orthorhombic
space group	$Pna2_1$ (no. 33)
unit cell dimens	a = 12.1025(4) Å
	b = 5.2676(1) Å
	c = 3.7132(1) Å
cell vol. (Å^3)	236.71(1)
density, calcd (g·cm^{-3})	2.793(1)

Analysis of the Average Long-Range Structure. The final refined structure of $CaSi_{1/3}B_{2/3}O_{8/3}$, containing one Ca, one Si/B mixed and three inequivalent O crystallographic sites all located on 4*a* positions, consists of linear chains parallel to the [001] direction (Figure 5). They are built up from distorted tetrahedra occupied by 1/3 (0.34(3)) silicon and 2/3 (0.66(3)) boron and are interconnected exclusively by O3 oxygen atoms.

dx.doi.org/10.1021/ic302114t | *Inorg. Chem.* 2013, 52, 4250−4258

Table 2. Atomic Coordinates and Anisotropic Atomic Displacement Parameters (ADP in Å^2) of $CaSi_{1/3}B_{2/3}O_{8/3}$ Determined from Rietveld Refinement of the Neutron Powder Diffraction (ILL-D2B) Pattern Collected at 650 °C[a]

atom	x	y	z	occupancy factor	B_{eq} (Å^2)
Ca	0.1498(3)	0.6047(7)	0.6140[b]	1	3,6(1)
Si	0.0899(2)	0.0854(5)	0.0970(30)	0.34(3)	3,6(1)
B	0.0899(2)	0.0854(5)	0.0970(30)	0.66(3)	3,6(1)
O1	0.1754(2)	0.9041(7)	0.1070(40)	1	4,6(1)
O2	0.1059(3)	0.3427(5)	0.0970(40)	1	6,9(2)
O3	0.9815(8)	0.0570(16)	0.2770(40)	0.634(8)	8,9(4)

atom	U_{11}	U_{22}	U_{33}	U_{12}	U_{13}	U_{23}
Ca	0.084(3)	0.0312(15)	0.021(2)	0.0158(17)	0.017(6)	0.002(5)
Si	0.041(3)	0.0216(16)	0.075(2)	0.0088(16)	−0.013(5)	0.001(6)
B	0.041(3)	0.0216(16)	0.075(2)	0.0088(16)	−0.013(5)	0.001(6)
O1	0.054(2)	0.0438(17)	0.077(3)	0.0204(18)	0.006(6)	−0.002(5)
O2	0.187(5)	0.0322(18)	0.044(2)	−0.008(2)	−0.029(7)	−0.006(5)
O3	0.060(6)	0.098(7)	0.179(10)	0.050(5)	0.034(6)	0.044(6)

[a]The structure is an average view integrated on several cells of the real local structure consisting of SiO_4 and BO_3 units arranged in short finite chains. This averaging leads to the large values of atomic displacement parameters, in particular, for the O3 oxygen. [b]Fixed value.

Table 3. Interatomic Distances for $CaSi_{1/3}B_{2/3}O_{8/3}$ Obtained from Rietveld Refinement of the Neutron Powder Diffraction (ILL-D2B) Pattern Collected at 650 °C

Si/B tetrahedron		Ca polyhedron	
Si/B−O1	1.409(4)	Ca−O1	2.475(11)
Si/B−O2	1.369(4)	Ca−O1	2.436(11)
Si/B−O3	1.478(12)	Ca−O1	2.364(5)
Si/B−O3	1.651(15)	Ca−O2	2.423(13)
		Ca−O2	2.325(13)
		Ca−O3	2.464(10)

The absence of approximately 1/3 oxygen on the O3 site in the cell, resulting of its partial occupancy (0.634(8)) determined by Rietveld refinement of neutron powder diffraction (Table 2), implies finite chains along the c axis. The calcium atom has a 5- or 6-fold coordination, sitting at the center of irregular CaO_6 polyhedra located around the tetrahedral chains.

The mean calcium−oxygen bond length of 2.41(6) Å (Table 3) is very close to those found in the danburite[6] ($CaB_2Si_2O_8$) and the okayamalite[8] ($Ca_2B_2SiO_7$) structures at 2.46 and 2.44 Å, respectively. However, the average bond distances calculated for the $[(Si_{1/3}B_{2/3})O_4]$ moieties in the $CaSi_{1/3}B_{2/3}O_{8/3}$ phase (1.48(4) Å) are shorter than the Si/B−O distance reported in the danburite (1.55 Å) and okayamalite (1.58 Å) minerals, the only calcium borosilicate phases referenced in the ICSD database. The mixed Si/B composition and partial O3 occupancy established for the average structure on the basis of long-range diffraction data lead to ambiguities in the description of the structure at the local level. Solid-state MAS NMR provides a complementary point of view on the local B and Si atomic environments present in the $CaSi_{1/3}B_{2/3}O_{8/3}$ phase.

Local Environments of Boron and Silicon. Solid-state ^{11}B NMR can be used as a direct local probe of the coordination state of the B atoms. The ^{11}B NMR echo-MAS spectrum of the $CaSi_{1/3}B_{2/3}O_{8/3}$ material is shown in black in Figure 6a. It is composed of a single resonance that can be modeled with a classical quadrupolar line shape with ^{11}B isotropic chemical shift (δ_{iso} = 19.5 ± 0.2 ppm), quadrupolar coupling constant (C_Q = 2.62 ± 0.05 MHz), and asymmetry parameter (η_Q = 0.51 ± 0.01) characteristic of a BO_3 moiety in a single crystallographic site, as shown in Figure 6a. Such a large

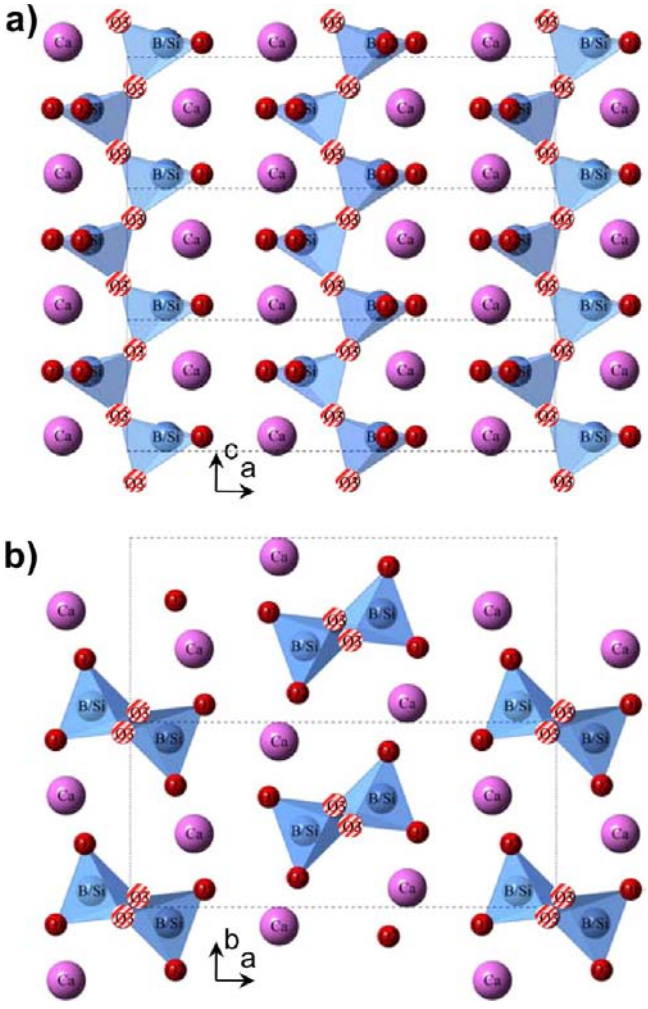

Figure 5. Projection of the $CaSi_{1/3}B_{2/3}O_{8/3}$ structure along the [010] (a) and [001] (b) directions obtained from Rietveld refinement from synchrotron and neutron powder diffraction data collected at high temperature. O3 oxygen atoms exhibiting partial occupancy (0.634(8)) are represented by hatched circles.

C_Q value reflects the anisotropic distribution of local charges and resulting electric field gradients (EFG) around a (nearly)

dx.doi.org/10.1021/ic302114t | Inorg. Chem. 2013, 52, 4250−4258

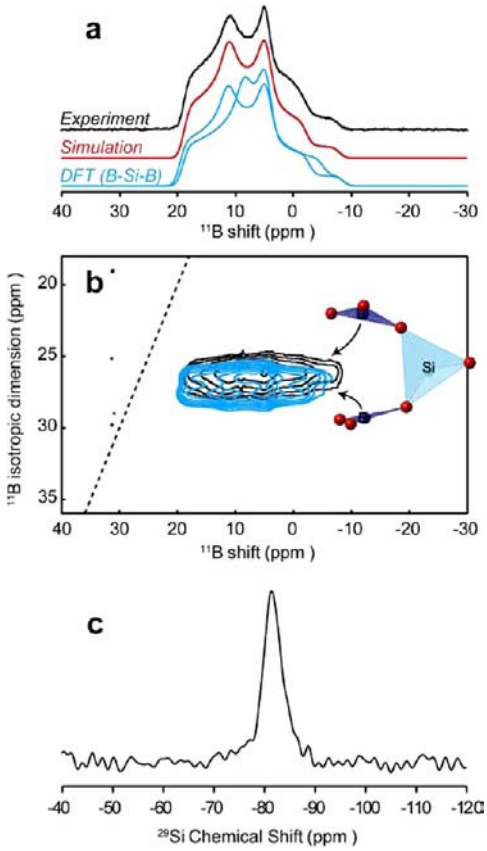

Figure 6. Solid-state NMR (a) ^{11}B echo-MAS, (b) ^{11}B multiple-quantum (MQ)-MAS, and (c) ^{29}Si single-pulse spectra (all in black) of $CaSi_{1/3}B_{2/3}O_{8/3}$, collected at room temperature, at magnetic fields of 9.4 T (for ^{11}B experiments) and 4.7 T (for ^{29}Si experiments). Simulated models are shown in red. ^{11}B NMR responses predicted with DFT calculations from local structural models containing "B−Si−B" units are shown in blue in a and b. (b) Representation of such local B−Si−B units, with BO_3 polyhedra in dark blue, SiO_4 tetrahedron in pale blue, and O atoms in red. Two slightly distinct individual contributions observed in a are reminiscent of the experimental distribution of ^{11}B shifts, as illustrated by their summed MQ-MAS contribution in b.

planar three-coordinated ^{11}B nucleus.[36,37] The measured asymmetry parameter η_Q = 0.51 representing the deviation of the EFG tensor from an axial symmetry points to BO_3 units connected to one or two nonbridging oxygen atoms (NBO)[38,39] rather than to isolated BO_3 units (with 3 NBO), an axially symmetric environment yielding η_Q values typically smaller than 0.3.[40] This spectrum establishes from a local point of view that the boron atoms all form BO_3 units (no detectable amount of four-coordinated B present) that correspond to chain ends along the *c* axis and are each systematically associated with an oxygen vacancy at one of the surrounding oxygen sites O3 along the chain. This implies that one of the next Si/B sites along the chain should also be occupied by a B atom to form a second BO_3 unit corresponding to the beginning of another chain along the *c* direction. Since the ^{11}B NMR data furthermore exclude the presence of isolated BO_3 units, such chains along the *c* axis should be of the form $O_2B-O-BO_2$ or $O_2B-O-[Si(O_2)-O-]_n-BO_2$ with $n \geq 1$ and silicon atoms in tetrahedral SiO_4 environments. For simplicity, these environments will be referred to thereafter as B−B, B−Si−B, B−Si−Si−B, ..., etc.

To increase spectral resolution and confirm the existence of a single rather than several possible BO_3 environments, a multiple-quantum (MQ)-MAS NMR experiment was conducted. Such experiments yield two-dimensional spectra in which the quadrupolar broadening is suppressed in the vertical dimension and lead to peak projections with line widths comparable to the spectra of spin-1/2 nuclei.[14] Figure 6b shows (in black) the ^{11}B MQ-MAS spectrum collected at room temperature for the $CaSi_{1/3}B_{2/3}O_{8/3}$ material. This 2D spectrum can be modeled (data not shown) with a single line with a similar set of parameters as extracted from the 1D ^{11}B echo-MAS NMR spectrum (Figure 6a), albeit with a distribution of ^{11}B shifts reflecting a certain degree of variability in the local bonding geometry and/or interchain arrangements. Because the positions of 2D NMR peaks in such MQ-MAS spectra strongly depend on δ_{iso}, C_Q, and η_Q, the probability that the signatures of two distinct molecular environments (such as B−B moieties and longer chains) may completely overlap is small. This suggests that the chains along the *c* axis are essentially composed by B−Si−B units as depicted in Figure 6b.

The ^{29}Si MAS NMR spectrum collected at room temperature (Figure 6c) is composed of a single line centered at ca. −81 ppm, consistent with the presence in the $CaSi_{1/3}B_{2/3}O_{8/3}$ material of a single type of local structural motif (B−Si−B moieties) giving rise to ^{29}Si nuclei connected via bridging O atoms to two three-coordinated B atoms, as highlighted from ^{11}B NMR results. These ^{29}Si environments are referred to thereafter as Si(2B). The signal is nevertheless slightly asymmetric and broadened at its base, pointing to an appreciable extent of local disorder attributed again to variations of the local bonding geometries and/or different interchain arrangements, for example.

Our interpretations of experimental ^{11}B and ^{29}Si NMR data can be verified on the basis of NMR parameters calculated by DFT. The models optimized by DFT (Figures 7a and Supporting Information, Figure 5) highlight the contrast

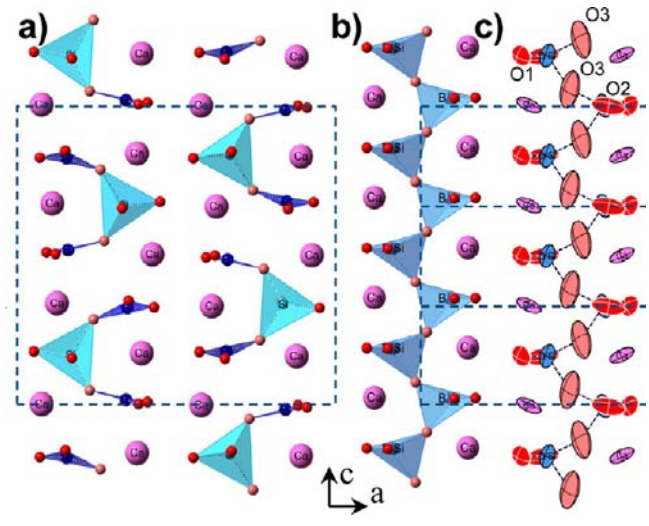

Figure 7. Representation of one of several possible polyhedral arrangements in Ca $Si_{1/3}B_{2/3}O_{8/3}$ along the *c* axis (a). Average structure obtained by high-temperature powder diffraction structure determination (b) is an average view of the proposed real structure represented on several cells, explaining the high values of atomic displacement parameters (c). Thermal ellipsoids are drawn at the 50% probability level.

dx.doi.org/10.1021/ic302114t | *Inorg. Chem.* 2013, 52, 4250−4258

Table 4. NMR Parameters Calculated by DFT for Models of the $CaSi_{1/3}B_{2/3}O_{8/3}$ Material

			^{29}Si NMR parameters[a]		^{11}B NMR parameters[a]		
supercell	calcd energy (eV)	local unit	site type	δ_{iso} (ppm)	δ_{iso} (ppm)	C_Q (MHz)	η_Q
$1 \times 1 \times 3$[b]	−27 550.18	B−Si−B	Si(2B)	−83.9	20.0(7)	2.68(6)	0.58(8)
$1 \times 1 \times 3$[c]	−27 550.10	B−Si−B	Si(2B)	−84.2	19.9(9)	2.66(6)	0.62(11)
$1 \times 1 \times 3$[c]	−27 549.93	B−B		N.A.	17.8(3)	2.55(2)	0.70(8)
		B−Si−B	Si(2B)	−84.0(5)	20.0(9)	2.67(8)	0.60(11)
		B−Si−Si−B	Si(1B)	−84.6(1)	21.1(1)	2.74(1)	0.50(2)
$1 \times 1 \times 6$[c]	−27 549.74[d]	B−Si−Si−Si−B	Si(0B)	−87.1			
			Si(1B)	−82(2)			
experimental[e]				−81(1)	19.5(2)	2.62(5)	0.51(1)

[a]Calculated NMR parameters are reported in the form $a \pm b$, where a is the average of the values calculated for all sites of a given type and b is the standard deviation among theses calculated values. [b]Model shown in Figure 7a, containing only B−Si−B units. [c]Models shown in Supporting Information, Figure SI5. [d]Scaled down (by a factor of 2) to the energy per $Ca_{12}Si_4B_8O_{32}$ unit for comparison with other systems. [e]Estimated uncertainties for the experimental parameters are indicated is parentheses.

between the local structure consisting of SiO_4 and BO_3 units and the structure determined by powder X-ray and neutron diffraction data (Figure 7b), which is an average view integrated over a vast number of cells. In particular, the $[(Si_{1/3}B_{2/3})O_4]$ tetrahedra in the average structure (in blue in Figure 7b) are highly distorted as a result, with large values of atomic displacement parameters, especially for the O3 oxygen (see Table 2 and thermal ellipsoids in Figure 7c).

NMR parameters calculated on the basis of these models confirm all of the interpretations and conclusions formulated above. Table 4 shows a summary of total energies, ^{29}Si δ_{iso} and ^{11}B δ_{iso}, C_Q, and η_Q calculated for the different structural models shown in Figure 7a and Supporting Information (Figure SI5). The model shown in Figure 7a and containing only B−Si−B units is the lowest in energy (although differences among the models are not much larger than our energy convergence criterion) and shows calculated ^{29}Si and ^{11}B NMR parameters all in good agreement with the experimental values. Importantly, this model is only one of several possible models based exclusively on B−Si−B units and differing by their interchain arrangements (see another example of such models in Figure SI5, Supporting Information), all of which may coexist in the room- and high-temperature structures.

Calculations of ^{29}Si chemical shifts do not rule out the presence of B−Si−Si−B units, whose predicted ^{29}Si shifts (Si(1B) at ca. −84 ppm) are very similar to those predicted for Si(2B) environments in B−Si−B units, suggesting that such moieties could be overlapping in the experimental spectrum. B−Si−Si−Si−B units, on the other hand, can be ruled out by ^{29}Si NMR calculations since the chemical shift predicted for the Si(0B) located at the center of such a chain (−87 ppm) is outside the observed range of experimental ^{29}Si chemical shifts. The absence (or negligible amount) of chains with more than one Si atom is deduced from calculations of ^{11}B NMR parameters. Calculations conducted on the different models containing exclusively B−Si−B units (Figure 7a, Supporting Information, Figure SI5a) each show two slightly distinct contributions for both sides of each chain (as shown in blue in Figure 6a and 6b for the model of Figure 7a) that are in good agreement with the 1D and 2D experimental spectrum and somewhat capture the distribution of ^{11}B shifts discussed above. The models shown in Figures 7a and SI5a, Supporting Information (data not shown), yield almost identical ^{11}B calculated spectra, illustrating that the ^{11}B parameters are in fact little affected by the interchain arrangement and directly reflect instead the type of local unit. In contrast, calculations conducted on models containing other local units predict that B−B units should be clearly separated from those of B−Si−B and longer chains in the ^{11}B MQ-MAS spectrum, if not in the ^{11}B 1D MAS NMR spectrum. ^{11}B peak positions predicted by DFT for B−B, B−Si−B, and B−Si−Si−B units contained in the model shown in Figure SI5b are displayed in the Supporting Information, Figure SI6. In light of these calculations, the observation of only a single type of ^{11}B environment experimentally further confirms that this material is primarily composed of B−Si−B units.

Existence of Ordering within the Calcium Borosilicate Phase at Room Temperature. As described above, electron diffraction analysis performed at room temperature provided approximate lattice parameters used to initially guide full determination of the high-temperature orthorhombic cell. At room temperature, however, extra reflections and weak diffuse streaks are observed in some areas of the crystals. In these regions, reconstruction of the reciprocal space reveals a supercell corresponding to a doubling of the cell determined previously along the a and b directions, leading to $a' = 2a \approx 24.2$ Å, $b' = 2b \approx 10.4$ Å, and $c' = c \approx 3.7$ Å. The absence of conditions limiting the general hkl reflections led to assignment of a primitive lattice, and systematic reflection conditions $0kl$, $k = 2n$, $h0l$, $h = 2n$, and $hk0$, $h + k = 2n$, were observed, suggesting the possible $Pban$ space group (Supporting Information, Figure SI4). The origin of the extra spots observed at room temperature may be clarified in light of a high-resolution transmission electron microscopy (HRTEM) investigation. The HRTEM image presented in Figure 8 is typical of a layered material with stacking along the a axis. Careful observation of the image, more particularly in the areas framed by the white squares, leads to identification of small domains exhibiting different contrasts related to specific atomic-scale arrangements of the material (highlighted by gray arrows on the image). Specifically, different arrangements of the bright dots can be noticed within the layers, leading to a doubling of the periodicity along a and b. The domains are about 10 nm large and correspond to a short-range ordering of the $CaSi_{1/3}B_{2/3}O_{8/3}$ phase at room temperature. This local ordering is confirmed by the apparition of extra reflections on the electron diffraction patterns calculated by Fourier transform from the HRTEM images of the selected areas. The nanometer size of these domains explains the broadening of the diffraction peaks observed at room temperature on the synchrotron and neutron powder diffraction data. This broadening prevents

dx.doi.org/10.1021/ic302114t | Inorg. Chem. 2013, 52, 4250−4258

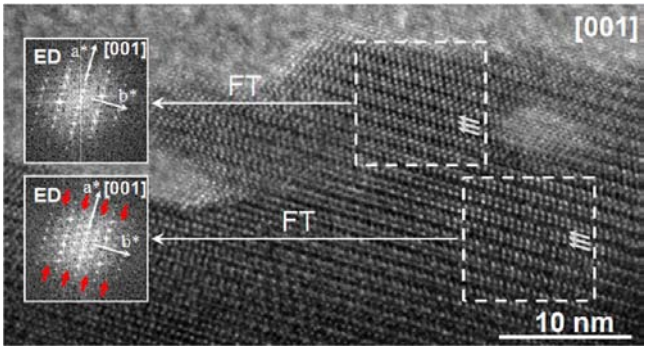

Figure 8. HREM image of $CaSi_{1/3}B_{2/3}O_{8/3}$ along the [001] axis zone, showing nanoscale domains with different layer stacking sequences at room temperature (gray arrows). Fourier transform (FT) patterns of these domains reveal the presence of extra reflections compared to the cell determined at high temperature. These reflections show the existence of a $2a \times 2b \times c$ structure at room temperature.

detection of very weak and similarly broadened superstructure peaks on room-temperature powder diffraction patterns.

The thermal dependence of this superstructure was investigated by in-situ electron diffraction study as a function of temperature. As shown in Figure 9, a progressive

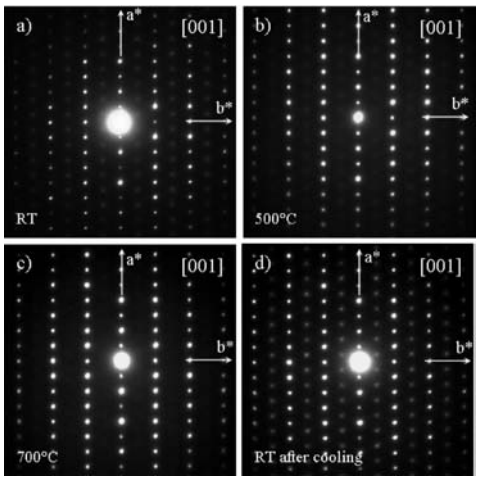

Figure 9. In-situ [001] electron diffraction patterns of the $CaSi_{1/3}B_{2/3}O_{8/3}$ sample at (a) room temperature, (b) 500 °C, (c) 700 °C, and (d) back to room temperature after heat treatment. Extra reflections disappear at high temperature but appear again upon cooling.

disappearance of the extra reflections present at room temperature and related to the superstructure on the [001] electron diffraction patterns can be observed with increasing temperature. This observation is consistent with the absence of superstructure peaks on high-temperature synchrotron and neutron diffraction diagrams (Figure 4) and suggests that the local ordering observed in $CaSi_{1/3}B_{2/3}O_{8/3}$ seems to be established only at low temperature. This slow transition is reversible, as established in Figure 9d by the reappearance of the superstructure peaks on the electron diffraction pattern collected after cooling the sample back to room temperature. Such ordering could result from interchain arrangements with adjacent B−Si−B units positioned differently at low temperature. These entities might well become mobile with increasing temperature, leading on average to identical adjacent chains and a 2-fold smaller unit cell in the a and b directions at 700 °C, where the structure could be determined.

CONCLUSION

This study evidences the existence of a new calcium borosilicate compound, $CaSi_{1/3}B_{2/3}O_{8/3}$, in the $CaO-SiO_2-B_2O_3$ ternary system that is of considerable interest to both the glass industry and the geological community. Synthesis of this new material was achieved by full crystallization from glass. Its crystal structure was solved ab initio from synchrotron and neutron powder diffraction data collected in situ at high temperature. The orthorhombic structure ($Pna2_1$, a = 12.1025(4) Å, b = 5.2676(1) Å, and c = 3.7132(1) Å) contains one Ca, one mixed Si/B, and three inequivalent O crystallographic sites located on 4a Wyckoff positions. Solid-state NMR spectroscopy has specified the local environments of both boron and silicon species, thus completing from a local point of view the description of this complex novel structure. It is composed of finite chains built up from SiO_4 tetrahedra and BO_3 trigonal planar coordination units along the [001] direction. The BO_3 units, corresponding to 2/3 of the mixed SiO_4/BO_3 polyhedra, are located at the end of the chains and correlated to the partial occupancy of the O3 oxygen. Combination of ^{11}B solid-state NMR and DFT calculations futhermore suggests that the $CaSi_{1/3}B_{2/3}O_{8/3}$ structure is essentially (if not only) composed of $BO_3-SiO_4-BO_3$ units. Finally, in-situ transmission electron microscopy revealed the presence of a reversible short-range ordering within nanometer domains at room temperature, which could be attributed to an ordering in interchain arrangements.

ASSOCIATED CONTENT

Supporting Information

$Ca_2Al_2SiO_7-Ca_2B_2SiO_7$ pseudo-binary phase diagram, DSC and variable-temperature XRD measurements of $2CaO-0.2Al_2O_3-0.8B_2O_3-SiO_2$ glass, TEM micrograph and corresponding EDS spectra of $CaO-0.2Al_2O_3-0.8B_2O_3-SiO_2$ bulk sample heated at 750 °C for 1 h and quenched to room temperature, XRD data recorded after crystallization at 750 °C of glasses with different boron contents, room-temperature ED patterns of the quenched $CaSi_{1/3}B_{2/3}O_{8/3}$ sample, additional DFT-optimized models discussed in the text, typical ^{11}B MQ-MAS signatures predicted by DFT, details of pseudopotentials used for DFT calculations, description of the model-building procedure, details of the chemical-shift referencing method for DFT calculations. This material is available free of charge via the Internet at http://pubs.acs.org.

AUTHOR INFORMATION

Corresponding Author

*E-mail: emmanuel.veron@cnrs-orleans.fr (E.V.); mathieu.allix@cnrs-orleans.fr (M.A.).

Notes

The authors declare no competing financial interest.

ACKNOWLEDGMENTS

We acknowledge financial support from the French CNRS (FR3507), CEA METSA network, and ANR (ANR-09-BLAN-0383-CSD 3). We thank the CRMD for TEM access and density measurements. Use of the Advanced Photon Source at Argonne National Laboratory was supported by the U.S.

Department of Energy, Office of Science, Office of Basic Energy Sciences, under contract No. DE-AC02-06CH11357.

REFERENCES

(1) Varshneya, A. K. *Fundamentals of Inorganic Glasses*; Academic Press: New York, 1994.
(2) Smedskjaer, M. M.; Mauro, J. C.; Youngman, R. E.; Hogue, C. L.; Potuzak, M.; Yue, Y. Z. *J. Phys. Chem. B* **2011**, *115* (44), 12930−12946.
(3) Ming, H.; Ren, Z. S.; Hua, Z. X. *J. Mater. Sci.-Mater. Electron.* **2011**, *22* (4), 389−393.
(4) Shao, H. B.; Wang, T. W.; Zhang, Q. T. *J. Alloys Compd.* **2009**, *484* (1−2), 2−5.
(5) Ryu, H. S.; Lee, J. K.; Seo, J. H.; Kim, H.; Hong, K. S.; Kim, D. J.; Lee, J. H.; Lee, D. H.; Chang, B. S.; Lee, C. K.; Chung, S. S. *J. Biomed. Mater. Res., Part A* **2004**, *68A* (1), 79−89.
(6) Phillips, M. W.; Gibbs, G. V.; Ribbe, P. H. *Am. Mineral.* **1974**, *59*, 79−85.
(7) Tarney, J.; Nicol, A. W.; Marriner, G. F. *Mineral. Mag.* **1973**, *39* (302), 158−175.
(8) Giuli, G.; Bindi, L.; Bonazzi, P. *Am. Mineral.* **2000**, *85* (10), 1512−1515.
(9) Fletcher, J. G.; Glasser, F. P. *J. Mater. Sci.* **1993**, *28* (10), 2677−2686.
(10) Suzuki, K. a. H. *J. Ceram. Assoc., Jpn.* **1970**, *78* (898), 189−195.
(11) Bauer, H. *Neues Jb. Miner. Monat.* **1962**, 127−140.
(12) Taylor, D. *Br. Ceram. Trans. J.* **1984**, *83* (4), 92−98.
(13) Iuga, D.; Kentgens, A. P. M. *J. Magn. Reson.* **2002**, *158* (1−2), 65−72.
(14) Frydman, L.; Harwood, J. S. *J. Am. Chem. Soc.* **1995**, *117* (19), 5367−5368.
(15) Amoureux, J. P.; Fernandez, C.; Steuernagel, S. *J. Magn. Reson., Ser. A* **1996**, *123* (1), 116−118.
(16) Massiot, D.; Fayon, F.; Capron, M.; King, I.; Le Calve, S.; Alonso, B.; Durand, J. O.; Bujoli, B.; Gan, Z. H.; Hoatson, G. *Magn. Reson. Chem.* **2002**, *40* (1), 70−76.
(17) Segall, M. D.; Lindan, P. J. D.; Probert, M. J.; Pickard, C. J.; Hasnip, P. J.; Clark, S. J.; Payne, M. C. *J. Phys.: Condens. Matter* **2002**, *14* (11), 2717−2744.
(18) Clark, S. J.; Segall, M. D.; Pickard, C. J.; Hasnip, P. J.; Probert, M. J.; Refson, K.; Payne, M. C. *Z. Kristallogr.* **2005**, *220* (5−6), 567−570.
(19) Perdew, J. P.; Burke, K.; Ernzerhof, M. *Phys. Rev. Lett.* **1996**, *77* (18), 3865−3868.
(20) Vanderbilt, D. *Phys. Rev. B* **1990**, *41* (11), 7892−7895.
(21) Profeta, M.; Benoit, M.; Mauri, F.; Pickard, C. J. *J. Am. Chem. Soc.* **2004**, *126* (39), 12628−12635.
(22) Sadoc, A.; Body, M.; Legein, C.; Biswal, M.; Fayon, F.; Rocquefelte, X.; Boucher, F. *Phys. Chem. Chem. Phys.* **2011**, *13* (41), 18539−18550.
(23) Pickard, C. J.; Mauri, F. *Phys. Rev. B* **2001**, *63* (24), 245101.
(24) Yates, J. R.; Pickard, C. J.; Mauri, F. *Phys. Rev. B* **2007**, *76* (2), 024401.
(25) Monkhorst, H. J.; Pack, J. D. *Phys. Rev. B* **1976**, *13* (12), 5188−5192.
(26) In *Powder Diffraction File*; Kabekkodu, S., Ed.; International Centre for Diffraction Data: Newtown Square, PA, USA, 2007.
(27) Stolyarova, V. L.; Lopatin, S. I.; Shugurov, S. M. *Russ. J. Gen. Chem.* **2008**, *78* (10), 1877−1881.
(28) Lebail, A.; Duroy, H.; Fourquet, J. L. *Mater. Res. Bull.* **1988**, *23* (3), 447−452.
(29) Palatinus, L.; Chapuis, G. *J. Appl. Crystallogr.* **2007**, *40*, 786−790.
(30) Petricek, V.; Dusek, M.; Palatinus, L. JANA2006. *The crystallographic computing system.*, **2006**.
(31) Oszlanyi, G.; Suto, A. *Acta Crystallogr., Sect. A* **2004**, *60*, 134−141.
(32) Liebau, F. *Structural Chemistry of Silicates*; Springer: Berlin, 1985.
(33) Thompson, P.; Cox, D. E.; Hastings, J. B. *J. Appl. Crystallogr.* **1987**, *20*, 79−83.
(34) Christ, C. L. *Am. Mineral.* **1959**, *44* (1−2), 176−177.
(35) Fleet, M. E. *Am. Mineral.* **1992**, *77* (1−2), 76−84.
(36) Smith, H. D.; Wiersema, R. J. *Inorg. Chem.* **1972**, *11* (5), 1152−1154.
(37) Turner, G. L.; Smith, K. A.; Kirkpatrick, R. J.; Oldfield, E. *J. Magn. Reson.* **1986**, *67* (3), 544−550.
(38) Kroeker, S.; Stebbins, J. F. *Inorg. Chem.* **2001**, *40* (24), 6239−6246.
(39) Konig, H.; Hoppe, R.; Jansen, M. *Z. Anorg. Allg. Chem.* **1979**, *449* (Feb), 91−101.
(40) Kriz, H. M.; Bray, P. J. *J. Magn. Reson.* **1971**, *4* (1), 76−84.